Robust Adaptive Control of Linear Induction Motors With Unknown End-Effect and Secondary Resistance

Kuang-Yow Lian, *Member, IEEE*, Cheng-Yao Hung, Chian-Song Chiu, *Member, IEEE*, and Li-Chen Fu, *Fellow, IEEE*

***Abstract*—This paper proposes a novel robust adaptive speed/position tracking control for a linear induction motor (LIM) with both end-effect and secondary resistance unknown. The practical current-fed controlled LIM, with residual current error, is considered, i.e., the traditional ideal current-loop assumption is relaxed. More practical conditions, such as bounded primary voltage and a finite absolute-integral of current tracking error is considered. To overcome the high nonlinearity and nonzero current error, a backstepping method, combining virtual desired variable synthesis, is developed for the speed and position tracking. Then, the controller achieves asymptotic speed and position tracking even with unknown parameters and immeasurable secondary flux. Furthermore, the effect of the residual current error is attenuated in an L_2-gain sense. The experiments for several scenarios are carried out to verify the theoretical result.**

***Index Terms*—Adaptive control, linear induction motors, position tracking, semi-current-fed model, speed tracking.**

I. Introduction

DUE TO HIGH starting thrust force, linear induction motors (LIMs) have been broadly used in industrial applications [1]–[5]. Compared to rotary induction motors (RIMs), the absence of leadscrews between LIMs and motion devices reduces mechanical losses, and lower noise. Although some literatures [5], [6] view the control problem of LIMs analogous to RIMs, the LIMs are more complicated due to: 1) end-effects are considered and dependent on the speed of the mover [7], [8]; and 2) larger electromechanical coupling constants. The end-effect is induced due to the unbalanced air gap flux occurring at both ends of the mover, which suppresses thrust force. Since the main thrust force decreases with increasing speed of the mover, the exact model is difficult to derive. In [9], a primary-flux-oriented control is proposed to improve the controller's robustness to variation of the secondary resistance. Thus, the end-effect and parametric uncertainties have not been considered together in previous literature [10], [11]. In addition, large electromechanical coupling constant leads to current-fed control [12], [13] failure since small current errors in the current loop may cause large force tracking errors and poor performance. The facts mentioned above motivate us to improve the control of LIMs.

In the control literature [12]–[18] of RIM, the controller design is usually based on reduced-order dynamics. This is the so-called current-fed RIM. Based on this concept, field-oriented control [14] and nonlinear decoupled control [15]–[18] are the main control methods. However, for LIMs, we can see that the current command and desired secondary fluxes can be independently designed using field-orientated control by a proper selection of state coordinates. Unfortunately, the ideal current loop is not satisfied easily in practical applications due to uncertainties and saturation. Furthermore, if the secondary flux is immeasurable, flux observer-based schemes (e.g., [19]–[21]) usually result in a complicated high-order control law. Therefore, for a practical current-fed inverter, immeasurable secondary flux, parametric uncertainties, and end-effects, lead to a challenging control of LIMs.

In this paper, we propose a robust adaptive control scheme for current-fed LIMs with practical current-loop constraints mentioned above. Therefore, in contrast to an ideal current-fed model, a relaxed version can be considered in this study (i.e., allowing nonzero current tracking error in the current loop). Hence the system will be called the *semi-current-fed LIM*. Although the dynamics of the current is considered, we only need to design a desired current as the control input (i.e., the controller is less complex and easier to be implemented). The end-effect of LIMs is modeled as an unknown external load force dependent on the mover speed. Next, a backstepping adaptive controller is developed to cope with the effect of nonzero current error and high coupling nonlinearity. To this end, virtual desired variables (VDVs) including virtual desired currents and fluxes are synthesized. Although we will treat the VDVs as desired variables to be tracked by the real current and flux, they need to be further defined indeed. This is why we call them as the *virtual* desired variables. Here, the immeasurable flux is adaptively reconstructed. If all mechanical parameters and partial electrical parameters are unknown, L_2-gain stability and asymptotic speed/position tracking are assured. The asymptotic flux tracking is achieved if the internal signals of the LIMs vary in a sufficiently rich manner (this is called persistent excitation (PE) condition [22]).

The rest of the paper is organized as follows. In Section II, we formulate the control problems of the practical current-fed controlled LIMs. In Section III, the VDV-based speed controller is derived. An extension to position control is addressed in Section IV. Section V shows the experimental results and

Manuscript received June 29, 2006; revised December 30, 2006. This work was supported by the National Science Council, R.O.C, under Grant NSC-93-2213-E-033-008. Paper no. TEC-00229-2006.

K.-Y. Lian is with the Department of Electrical Engineering, National Taipei University of Technology, Taipei 10608, Taiwan (e-mail: kylian@ntut.edu.tw).

C.-Y. Hung is with the Department of Electrical Engineering, Chung-Yuan Christian University, Chung-Li 32023, Taiwan, R.O.C.

C.-S. Chiu is with the Department of Electrical Engineering, Chung-Yuan Christian University, Chung-Li 32023, Taiwan, R.O.C (e-mail: cschiu@dec.ee.cycu.edu.tw).

L.-C. Fu is with the Department of Electrical Engineering, National Taiwan University, Taipei 10617, Taiwan, R.O.C. (e-mail: lichen@ccms.ntu.edu.tw).

Digital Object Identifier 10.1109/TEC.2007.905058

comparisons of the proposed and traditional controllers. Finally, some conclusions are made in Section VI.

II. Problem Formulation

Denoting the state vectors $\mathbf{i} = [i_{pa} \quad i_{pb}]^\top$, $\lambda = [\lambda_{sa} \quad \lambda_{sb}]^\top$, and $\mathbf{V}_p = [V_{pa} \ V_{pb}]^\top$, the fifth-order dynamic model of the LIM in *a, b* stationary reference frame is described by the following vector compact form [1], [3], [21]:

$$\sigma\dot{\mathbf{i}} = -\left(\frac{L_s R_p}{L_m} + \frac{L_m R_s}{L_s}\right)\mathbf{i} - \left(\frac{\pi}{\ell} n_p v_m \mathbf{J}_2 - \frac{R_s}{L_s}\mathbf{I}_2\right)\lambda + \frac{L_s}{L_m}\mathbf{V}_p \tag{1}$$

$$\dot{\lambda} = \frac{L_m R_s}{L_s}\mathbf{i} + \left(\frac{\pi}{\ell} n_p v_m \mathbf{J}_2 - \frac{R_s}{L_s}\mathbf{I}_2\right)\lambda \tag{2}$$

$$M\dot{v}_m = F - F_l - D v_m \tag{3}$$

and

$$\mathbf{I}_2 = \begin{bmatrix} 1 & 0 \\ 0 & 1 \end{bmatrix} \text{ and } \mathbf{J}_2 = \begin{bmatrix} 0 & -1 \\ 1 & 0 \end{bmatrix}$$

where

σ	$= L_s L_p / L_m - L_m$;
F	$= \kappa \mathbf{i}^\top \mathbf{J}_2 \lambda$;
κ	$= 3\pi n_p L_m / 2\ell L_s$;
$i_{pa}(i_{pb})$	a-axis and b-axis primary current;
$V_{pa}(V_{pb})$	a-axis and b-axis primary voltage;
$\lambda_{sa}(\lambda_{sb})$	a-axis and b-axis secondary flux;
v_m	mover speed;
$R_p(R_s)$	primary (secondary) resistance;
$L_p(L_s)$	primary (secondary) inductance;
L_m	mutual inductance;
ℓ	pole pitch;
M	primary mass;
D	viscous friction;
n_p	number of pole pairs;
F_l	load disturbance;
F	electromechanical coupling force;
κ	force constant.

Throughout this study, we assume that the parameters R_p, L_p, L_s, and L_m are known constants whereas R_s, M, and D are unknown constants. The longitudinal end-effect is approximated by Taylor's series and can be taken as an external load force

$$F_l = \theta_1 + \theta_2 v_m + \theta_3 v_m^2 \tag{4}$$

with unknown constants θ_1, θ_2, and θ_3 [6]. This end-effect increases with the speed of the primary [7], [8].

Due to the limitation of the electromagnetic path of LIM, the mutual flux between the primary and secondary will saturate easily if high-gain current-loop control is used. For these reasons, it is impractical to adopt the ideal current loop model, where zero current tracking error is assumed. In other words $\mathbf{i}$ in (2) cannot be directly replaced by the desired control input $\mathbf{i}^*$. Thus, the control problem of a practical current-fed LIM is formulated as shown in the next subsection.

A. Robust Semi-Current-Fed LIM Control Problem

Consider an LIM driven by the PI current control law

$$\mathbf{V}_p = -K_p(\mathbf{i} - \mathbf{i}^*) - K_i \int_0^t (\mathbf{i} - \mathbf{i}^*) d\tau \tag{5}$$

where K_p and K_i are proper loop gains. If the current loop performs well and provides a bounded $\mathbf{V}_p$ (i.e., $(\mathbf{i} - \mathbf{i}^*) \in L_\infty$), how will the desired current $\mathbf{i}^*$ be properly designed such that the closed-loop system satisfies the performance criterion

$$\int_0^t \|\mathbf{e}(\tau)\|^2 d\tau \le \epsilon_1 + \epsilon_2 \int_0^t \|\widetilde{\mathbf{i}}(\tau)\|^2 d\tau \tag{6}$$

with $\epsilon_1, \epsilon_2 > 0$, as tunable parameters and $\widetilde{\mathbf{i}} = \mathbf{i} - \mathbf{i}^*$? Note that $\mathbf{e}(t)$ consists of speed, position, or flux tracking errors.

B. Asymptotic Semi-Current-Fed LIM Control Problem

Consider a LIM driven by the PI current control law (5). If the current controller (5) assures a bounded $\mathbf{V}_p$ and a finite integrable current tracking error $\widetilde{\mathbf{i}}$, how will the desired current $\mathbf{i}^*$ be properly designed such that the control error $\mathbf{e}(t)$ asymptotically converges to zero? In the above, the semi-current-fed LIM means that the LIM is driven by a well-performed current loop but the current error $\widetilde{\mathbf{i}}(t)$ is not negligible. This new concept preserves the benefit (i.e., a reduced model-based design) of traditional current-fed control while considering practical situations.

Since the current error is not negligible, field oriented control and vector control is hard to implement. Therefore, we introduce a new design in the next section.

III. VDV-Based Speed Control

Assume that the primary current, voltages, and mover speed are measurable (but the flux is unmeasurable). The control objective is to track a desired speed v_d which satisfies $v_d, \dot{v}_d \in L_\infty$. The controller is synthesized by three steps—mechanical loop control, electrical loop control, and an adaptive mechanism described below.

A. Mechanical Loop Control

First, consider the mechanical dynamics (3) and denote the speed tracking error as $\tilde{v}_m = v_m - v_d$. The error dynamics of $\tilde{v}_m$ can be written as

$$M\dot{\tilde{v}}_m + (D + k_v)\tilde{v}_m = F - F_d + (F_d - \mathbf{Y}\theta + k_v \tilde{v}_m)$$

where F_d denotes a VDV for the electromechanical coupling force $F, k_v > 0$ is an adjustable damping ratio; $\mathbf{Y} = [1 \quad v_m \quad v_m^2 \quad v_d \quad \dot{v}_d]$ is a regression matrix; $\theta = [\theta_1 \quad \theta_2 \quad \theta_3 \quad D \quad M]^\top$ is an unknown parametric vector; and the expression (4) has been used. To provide the desired speed, we set the virtual desired force

$$F_d = \mathbf{Y}\widehat{\theta} - k_v \tilde{v}_m, \tag{7}$$

where $\widehat{\theta}$ is the estimated vector of θ. This yields the error dynamics

$$M\dot{\tilde{v}}_m + (D + k_v)\,\tilde{v}_m = F - F_d - \mathbf{Y}\widetilde{\theta} \tag{8}$$

with the estimation error $\widetilde{\theta} \equiv \theta - \widehat{\theta}$.

At this point, the speed tracking control problem has been transformed into a force tracking problem. The remainder of the control design is to let the electrical loop of the LIM to generate the desired force F_d.

B. Electrical Loop Control

Next, consider the electrical dynamics (1) and (2). The following design scheme is somewhat similar to the well-known backstepping control [23]. However, for our problem, direct implementation of backstepping control is not trivial due to the highly coupled nonlinearity of the LIM. To cope with this, two other VDVs $\mathbf{i}^*$ and λ_d are introduced for $\mathbf{i}$ and λ. Indeed, the VDV $\mathbf{i}^*$ is the desired current to be taken as an input of the current loop (5). The VDV λ_d is the desired flux for generating the optimal force. Meanwhile, the desired current $\mathbf{i}^*$ and desired flux λ_d are designed such that the electrical subsystem provides the desired force F_d.

To this end, let VDVs $\mathbf{i}^*$ and λ_d satisfy

$$F_d = \kappa \mathbf{i}^{*\top}\mathbf{J}_2\lambda_d. \tag{9}$$

This means that F converges to F_d once $\mathbf{i}$ and λ converge to $\mathbf{i}^*$ and λ_d, respectively. The convergence of $\mathbf{i}$ to $\mathbf{i}^*$ depends on the performance of the current loop controller. However, the objective of $\lambda \to \lambda_d$ is achieved by an appropriate choice of $\mathbf{i}^*$ from (2). As a result, $\mathbf{i}^*$ will be properly designed such that $\lambda \to \lambda_d$ while satisfying (9).

To generate the optimal force, the virtual desired flux in the primary-fixed frame is set in the form:

$$\lambda_d = \begin{bmatrix} c\cos(\rho(t)) \\ c\sin(\rho(t)) \end{bmatrix}, \tag{10}$$

where $c = \|\lambda_d\|$ is the magnitude of the desired secondary flux; and $\rho(t)$ denotes the electrical angle with respect to the primary-fixed frame, to be determined later. Next, we attempt to design $\mathbf{i}^*$ and $\rho(t)$ such that $\lambda \to \lambda_d$ under the constraint (9).

Since the secondary flux is immeasurable, the direct error-feedback approach is not possible. To solve this problem and avoid using a flux observer, an alternative flux reconstruction is derived here. By adding (1) and (2), we obtain that

$$\sigma\dot{\mathbf{i}} + \dot{\lambda} = \dot{\eta} \tag{11}$$

with the first-order filter

$$\dot{\eta} = -\frac{L_s R_p}{L_m}\mathbf{i} + \frac{L_s}{L_m}\mathbf{V}_p. \tag{12}$$

By integrating (11), the flux can be represented as

$$\lambda = \eta - \sigma\mathbf{i} + \mathbf{c}_0 \tag{13}$$

where η is the output of the filter (12); and $\mathbf{c}_0$ is an unknown integration constant vector dependent on initial conditions. From (13), the flux is reconstructed in the form: $\widehat{\lambda} = \eta - \sigma\mathbf{i} + \widehat{\mathbf{c}}_0$ with the estimation $\widehat{\mathbf{c}}_0$ for $\mathbf{c}_0$.

The filter (12) can be further represented as a stable filter:

$$\dot{\eta} = -\frac{L_s R_p}{L_m\sigma}\eta + \frac{L_s R_p}{L_m\sigma}(\lambda - \mathbf{c}_0) + \frac{L_s}{L_m}\mathbf{V}_p \tag{14}$$

where the relation (13) has been applied. Hence, the effect due to the unknown initial value of $\eta(t)$ will fade out. In addition, if the offsets in current and voltage measurements are present, these offsets can be contained in $\mathbf{c}_0$ and coped by the adaptive technique. Thus, the proposed flux reconstruction is suitable for practical implementation.

To proceed further, we change the original flux tracking into the tracking of reconstructed flux $\widehat{\lambda}$ to λ_d. Defining the new tracking error as $\widetilde{\lambda} = \widehat{\lambda} - \lambda_d$, we obtain

$$\begin{aligned}\dot{\widetilde{\lambda}} = &\left(\frac{\pi}{\ell}n_p v_m\mathbf{J}_2 - \frac{R_s}{L_s}\mathbf{I}_2 - \frac{R_s L_m k_{\boldsymbol{\lambda}}}{L_s}\mathbf{I}_2\right)\widetilde{\lambda} + \widetilde{R}_s\phi_r \\ &+ \frac{\pi}{\ell}n_p v_m\mathbf{J}_2\widetilde{\mathbf{c}}_0 - \widetilde{\vartheta} + \frac{L_m R_s}{L_s}\widetilde{\mathbf{i}} + \xi_{\boldsymbol{\lambda}} - \tau_a,\end{aligned} \tag{15}$$

where $\xi_{\boldsymbol{\lambda}} = (\frac{\pi}{\ell}n_p v_m\mathbf{J}_2 - \frac{\widehat{R}_s}{L_s}\mathbf{I}_2)\lambda_d + \frac{L_m\widehat{R}_s}{L_s}k_{\boldsymbol{\lambda}}\widetilde{\lambda} - \widehat{\vartheta} + \frac{\widehat{R}_s}{L_s}\widehat{\mathbf{c}}_0 + \frac{L_m}{L_s}\widehat{R}_s\mathbf{i}^* + \dot{\widehat{\mathbf{c}}}_0 - \dot{\lambda}_d + \tau_a$ and $\phi_r = \frac{L_m}{L_s}\mathbf{i}^* - \frac{1}{L_s}\lambda_d + \frac{1}{L_s}\widehat{\mathbf{c}}_0 + \frac{L_m}{L_s}k_{\boldsymbol{\lambda}}\widetilde{\lambda}$. The detailed derivation is given in Appendix I. In the above, $\widehat{R}_s$ is the estimated secondary resistance; $\widetilde{R}_s = R_s - \widehat{R}_s$ is the estimation error; $\widehat{\vartheta}$ is the estimated signal of $\vartheta \equiv \frac{R_s}{L_s}\mathbf{c}_0$; $\widetilde{\vartheta} = \vartheta - \widehat{\vartheta}$ is the estimation error; $\widetilde{\mathbf{c}}_0 = \mathbf{c}_0 - \widehat{\mathbf{c}}_0$; $k_{\boldsymbol{\lambda}} > 0$ is a control gain; and τ_a is an auxiliary signal determined later. In (15), we take $\xi_{\boldsymbol{\lambda}}$ as a perturbation term and set $\xi_{\boldsymbol{\lambda}} = 0$ to determine $\mathbf{i}^*$ and $\rho\,(t)$. According to the conditions $\xi_{\boldsymbol{\lambda}} = 0$, (9) and $\dot{\lambda}_d = \dot{\rho}\,(t)\,\mathbf{J}_2\lambda_d$, we obtain

$$\begin{aligned}\mathbf{i}^* = &\frac{1}{L_m}\left(\mathbf{I}_2 + \frac{1}{c^2}\psi\mathbf{J}_2\right)\lambda_d + \frac{L_s}{L_m\widehat{R}_s}(\widehat{\vartheta} - \dot{\widehat{\mathbf{c}}}_0 - \tau_a) \\ &- k_{\boldsymbol{\lambda}}\widetilde{\lambda} - \frac{1}{L_m}\widehat{\mathbf{c}}_0,\end{aligned} \tag{16}$$

$$\dot{\rho}\,(t) = \frac{\pi}{\ell}n_p v_m + \frac{\widehat{R}_s}{c^2 L_s}\psi, \tag{17}$$

where $\psi = \frac{L_m F_d}{\kappa} + (L_m k_{\boldsymbol{\lambda}}\widetilde{\lambda} + \widehat{\mathbf{c}}_0 + \frac{L_s}{\widehat{R}_s}(\dot{\widehat{\mathbf{c}}}_0 + \tau_a - \widehat{\vartheta}))^\top\mathbf{J}_2\lambda_d$. Obviously, the estimation $\widehat{R}_s(t) \neq 0$ is needed for all t, which will be achieved by a proper adaptive mechanism. Hence, the design of λ_d and $\mathbf{i}^*$ have been completed.

C. Adaptive Mechanism

Now, we are going to derive the update laws for all parameter estimations. Based on the control law (5) with the desired current (16), the error dynamics (8) and (15) are further expressed as

$$M\dot{\tilde{v}}_m + (D + k_v)\tilde{v}_m = \kappa(\mathbf{i}^\top\mathbf{J}_2\widetilde{\lambda} + \mathbf{i}^\top\mathbf{J}_2\widetilde{\mathbf{c}}_0 + \widetilde{\mathbf{i}}^\top\mathbf{J}_2\lambda_d) - \mathbf{Y}\widetilde{\theta} \tag{18}$$

$$\begin{aligned}\dot{\widetilde{\lambda}} = &\left(\frac{\pi}{\ell}n_p v_m\mathbf{J}_2 - \frac{R_s(1 + L_m k_{\boldsymbol{\lambda}})}{L_s}\mathbf{I}_2\right)\widetilde{\lambda} \\ &+ \widetilde{R}_s\phi_r + \frac{\pi}{\ell}n_p v_m\mathbf{J}_2\widetilde{\mathbf{c}}_0 - \widetilde{\vartheta} + \frac{L_m R_s}{L_s}\widetilde{\mathbf{i}} - \tau_a\end{aligned} \tag{19}$$

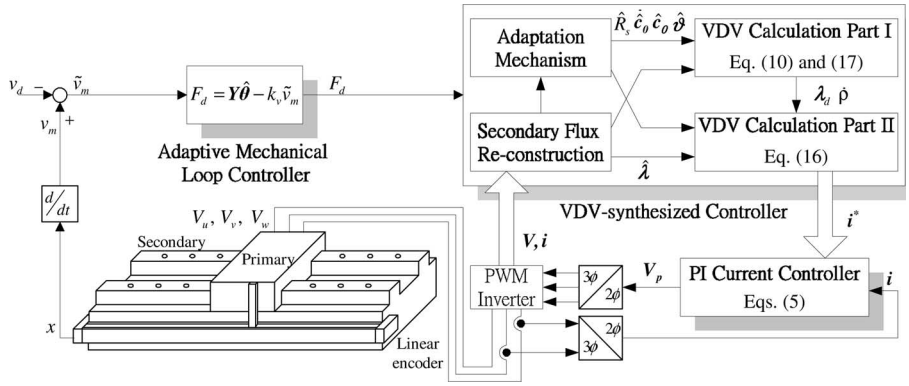

Fig. 1. Structure of the adaptive speed controller.

where the current error $\widetilde{\mathbf{i}}$ appears in the error dynamics since a semi-current-fed LIM is considered. Accordingly, update laws of $\widehat{R}_s, \widehat{\theta}, \widehat{\mathbf{c}}_0$ and $\widehat{\vartheta}$ are suitably chosen for (18) and (19) such that the tracking errors $\tilde{v}_m$ and $\widetilde{\lambda}$ are convergent. To this end, let us consider a Lyapunov function candidate as

$$V = \frac{1}{2}\big(\alpha M\tilde{v}_m^2 + \alpha\widetilde{\theta}^\top\mathbf{\Gamma}_1^{-1}\widetilde{\theta} + \widetilde{\lambda}^\top\widetilde{\lambda} + \gamma_s^{-1}\widetilde{R}_s^2 + \widetilde{\mathbf{c}}_0^\top\mathbf{\Gamma}_2^{-1}\widetilde{\mathbf{c}}_0 + \widetilde{\vartheta}^\top\mathbf{\Gamma}_3^{-1}\widetilde{\vartheta}\big) \tag{20}$$

where α is an arbitrary positive constant; and $\gamma_s, \mathbf{\Gamma}_1 = \mathbf{\Gamma}_1^\top$, $\mathbf{\Gamma}_2 = \mathbf{\Gamma}_2^\top, \mathbf{\Gamma}_3 = \mathbf{\Gamma}_3^\top$ are positive definite adaptation gains. The time derivative of (20) along the error dynamics (18) and (19) is

$$\begin{aligned}\dot{V} = &-\alpha(D+k_v)\tilde{v}_m^2 + \alpha\widetilde{\theta}^\top\big(\mathbf{\Gamma}_1^{-1}\dot{\widetilde{\theta}} - \tilde{v}_m\mathbf{Y}^\top\big)\\ &- \frac{R_s}{L_s}(1+L_m k_\lambda)\widetilde{\lambda}^\top\widetilde{\lambda} + \widetilde{R}_s\big(\gamma_s^{-1}\dot{\widetilde{R}}_s + \widetilde{\lambda}^\top\phi_r\big)\\ &+ \widetilde{\mathbf{c}}_0^\top\big(\mathbf{\Gamma}_2^{-1}\dot{\widetilde{\mathbf{c}}}_0 + \alpha\kappa\tilde{v}_m\mathbf{J}_2^\top\mathbf{i} + \frac{\pi}{\ell}n_p v_m\mathbf{J}_2^\top\widetilde{\lambda}\big)\\ &+ \widetilde{\vartheta}^\top\big(\mathbf{\Gamma}_3^{-1}\dot{\widetilde{\vartheta}} - \widetilde{\lambda}\big) + \widetilde{\lambda}^\top\big(\alpha\kappa\tilde{v}_m\mathbf{J}_2^\top\mathbf{i} - \tau_a\big)\\ &+ \widetilde{\mathbf{i}}^\top\big(\alpha\kappa\tilde{v}_m\mathbf{J}_2\lambda_d + \frac{L_m R_s}{L_s}\widetilde{\lambda}\big).\end{aligned}$$

Therefore, the update laws for $\widehat{R}_s, \widehat{\theta}, \widehat{\mathbf{c}}_0$ and $\widehat{\vartheta}$ are respectively chosen as

$$\dot{\widehat{\theta}} = -\tilde{v}_m\mathbf{\Gamma}_1\mathbf{Y}^\top \tag{21}$$

$$\dot{\widehat{\mathbf{c}}}_0 = \mathbf{\Gamma}_2\left(\alpha\kappa\tilde{v}_m\mathbf{J}_2^\top\mathbf{i} + \frac{\pi}{\ell}n_p v_m\mathbf{J}_2^\top\widetilde{\lambda}\right) \tag{22}$$

$$\dot{\widehat{\vartheta}} = -\mathbf{\Gamma}_3\widetilde{\lambda} \tag{23}$$

$$\dot{\widehat{R}}_s = \begin{cases} 0, & \text{if } \widehat{R}_s = R_0 \text{ and } \widetilde{\lambda}^\top\phi_r < 0 \\ \gamma_s\widetilde{\lambda}^\top\phi_r, & \text{otherwise} \end{cases} \tag{24}$$

with the initial condition $\widehat{R}_s(0) > R_0$, where R_0 denotes a lower bound of the unknown secondary resistance R_s. Note that the update law for the estimation $\widehat{R}_s$ guarantees $\widehat{R}_s(t) > R_0$ and $\widetilde{R}_s(\gamma_s^{-1}\dot{\widetilde{R}}_s + \widetilde{\lambda}^\top\phi_r) \le 0$ for all t. However, the auxiliary signal τ_a in (15) is obtained as

$$\tau_a = \alpha\kappa\tilde{v}_m\mathbf{J}_2^\top\mathbf{i}.$$

As a result, the time derivative of V leads to

$$\dot{V} \le -\alpha(D+k_v)\tilde{v}_m^2 - \frac{R_s}{L_s}\left(1+L_m k_\lambda\right)\widetilde{\lambda}^\top\widetilde{\lambda} + \widetilde{\mathbf{i}}^\top\begin{bmatrix}\alpha\kappa\mathbf{J}_2\lambda_d & \dfrac{L_m R_s}{L_s}\mathbf{I}_2\end{bmatrix}\begin{bmatrix}\tilde{v}_m \\ \widetilde{\lambda}\end{bmatrix}. \tag{25}$$

The overall structure of the control law along with the update laws are illustrated in Fig. 1. Obviously, the convergence of $\tilde{v}_m$ and $\widetilde{\lambda}$ is dependent on the residual current error $\widetilde{\mathbf{i}}$ which exists in practical current-fed control (i.e., $\widetilde{\mathbf{i}} = 0$ for an ideal current-fed control).

D. Main Results

First, the robust semi-current-fed LIM speed control problem is solved below.

1) Result for the Robust Speed Control: Consider the virtual desired force, flux, and current, accordingly, addressed in (7), (10), and (16) along with update laws (21)–(24). If the control gains satisfy

$$\alpha > 0 \tag{26}$$

$$D + k_v - \frac{\kappa c^2}{4R_s} > 0 \tag{27}$$

$$1 + L_m k_\lambda - \frac{L_m^2}{4L_s\alpha} > 0 \tag{28}$$

and current loop gains K_p, K_i are properly chosen such that $\mathbf{V}_p \in L_\infty$, then the robust semi-current-fed LIM speed control problem is solved. The closed-loop system has all bounded signals and achieves the performance criterion (6) with $\mathbf{e}(t) = [\tilde{v}_m \;\; \widetilde{\lambda}^\top]^\top$. □

The proof of this result is given in Appendix II. If the current-loop controller (5) performs very well and assures $\mathbf{V}_p \in L_\infty$ and $\widetilde{\mathbf{i}} \in L_1$, we have $\widetilde{\mathbf{i}} \in L_2$. In light of this result, we have $\mathbf{e} \in L_2$ by (6). In addition, the fact $\dot{\mathbf{e}} \in L_\infty$ is concluded since all signals on the right-hand sides of (18) and (19) are bounded. According to $\mathbf{e}, \dot{\mathbf{e}} \in L_\infty, \mathbf{e} \in L_2$ and applying Barbalat's lemma [22], we have $\lim_{t\to\infty}\mathbf{e}(t)$. In other words, $\tilde{v}_m$ and $\widetilde{\lambda}$ asymptotically converge to zero as $t \to \infty$. Hence, the asymptotic semi-current-fed LIM speed control problem is solved below.

2) Result for the Asymptotic Speed Control: Consider the virtual desired force, flux, and current, accordingly, addressed in (7), (10), and (16) along with update laws (21)–(24). If the control gains satisfy (26)–(28) and the current loop gains K_p, K_i are properly chosen such that $\mathbf{V}_p \in L_\infty$ and $\widetilde{\mathbf{i}} \in L_1$, then asymptotic semi-current-fed LIM speed control is achieved, i.e., $\lim_{t\to\infty} \tilde{v}_m(t) = 0$ and $\lim_{t\to\infty} \widetilde{\lambda}(t) = 0$. □

From the robust speed control, the tracking errors $\tilde{v}_m$ and $\widetilde{\lambda}$ with respect to the current error $\widetilde{\mathbf{i}}$ are finite-gain L_2 stable for a practical current-fed LIM. For zero-state response, we have

$$\epsilon_Q \|\mathbf{e}(t)\|_2 \le \alpha R_s(\kappa+1)\|\widetilde{\mathbf{i}}(t)\|_2$$

with $\epsilon_Q = \|\mathbf{Q}\|$ and $\mathbf{Q}$ in defined in Appendix II, which means that the effect of the residual current error $\widetilde{\mathbf{i}}(t)$ on the tracking error $\mathbf{e}(t)$ is dependent on the parameters α, R_s, and κ. Usually, the electromechanical coupling constant κ of LIMs is much larger than the value of RIM. This means that the control performance of LIM is easily affected by the current error when compared with RIM. From the above analysis, the proposed scheme attenuates the effect of the residual current error by control gain α. Therefore, we are able to obtain an expected control performance by properly tuning the control gains $k_v, k_{\boldsymbol{\lambda}}$, and α even if the current-control loop does not work well.

Notice that, $\tilde{v}_m$ and $\widetilde{\lambda}$ converge to zero asymptotically as $t \to \infty$ without needing the PE condition. If the internal signals are persistently excited, the secondary flux tracking error $(\boldsymbol{\lambda} - \boldsymbol{\lambda}_d)$ asymptotically converges to zero. Since the secondary flux tracking error $(\boldsymbol{\lambda} - \boldsymbol{\lambda}_d)$ equals to $(\widetilde{\lambda} + \widetilde{\mathbf{c}}_0)$, we need $\widetilde{\mathbf{c}}_0 \to 0$ to achieve $\boldsymbol{\lambda} \to \boldsymbol{\lambda}_d$ as $t \to \infty$. In traditional adaptive approaches [22], zero parameter errors are obtained only if the PE condition is satisfied. Let

$$\mathbf{W}^\top(t) = \begin{bmatrix} -\alpha\mathbf{Y} & \alpha\kappa\mathbf{i}^\top\mathbf{J}_2 & 0 & 0 \\ 0 & \frac{\pi}{\ell} n_p v_m \mathbf{J}_2 & -\mathbf{I}_2 & \phi_r \end{bmatrix}.$$

If $\mathbf{W}(t)$ satisfies the PE condition, i.e., there exist two positive constants ν and μ such that

$$\int_t^{t+\nu} \mathbf{W}(\tau)\mathbf{W}^\top(\tau)\,d\tau \ge \mu\mathbf{I} > 0, \forall t \ge 0,$$

then asymptotic flux tracking will be achieved, that is, $\lim_{t\to\infty}(\boldsymbol{\lambda} - \boldsymbol{\lambda}_d) = 0$. Therefore, the optimal force property will be sustained if the PE condition is satisfied.

IV. Position Controller Design

Based on the proposed speed control in the above section, the block diagram of the position control design for the LIM is formulated in Fig. 2. The position control is regarded as another external control loop, i.e., the signal v_d becomes a VDV for the speed-control loop. Therefore, we only need to design the virtual desired speed v_d at this step.

Let us consider the desired position x_d, its time derivative $\dot{x}_d$, and its second-order time derivative $\ddot{x}_d$ as bounded functions. Denote the position tracking error as $\tilde{x} = x - x_d$ and let the virtual desired speed be:

$$v_d = \dot{x}_d - k_x\tilde{x} \tag{29}$$

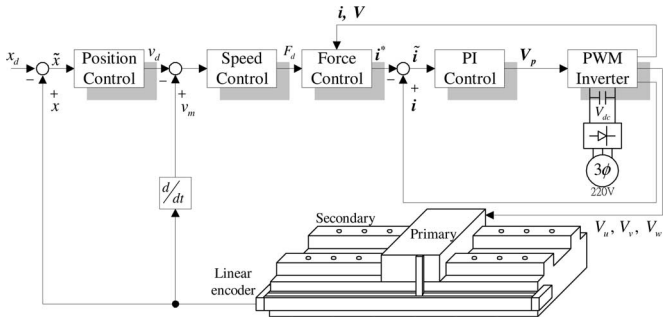

Fig. 2. Concept of position control design for semi-current-fed linear induction motor.

with $k_x > 0$. This yields the position error dynamics $\dot{\tilde{x}} + k_x\tilde{x} = \tilde{v}_m$. Thus, the position tracking error $\tilde{x}$ converges to zero as long as $\lim_{t\to\infty}\tilde{v}_m = 0$. Compared to (7), we further modify the force command as

$$F_d = \mathbf{Y}\widehat{\theta} - k_v\tilde{v}_m - \tilde{x}. \tag{30}$$

Then, the remainder of the design is the same as the design procedure addressed in Section III-B and III-C. Furthermore, the stability can be obtained by considering the Lyapunov function $V_x = \frac{1}{2}\alpha\tilde{x}^2 + V$. As a result, we give the following result for the position tracking control of a practical LIM.

A. Result for the Position Tracking Control

Consider the virtual desired speed, force, flux, and current, accordingly, addressed in (29), (30), (10), and (16) along with update laws (21)–(24), where the control gains satisfy $k_x > 0$, and (26)–(28). If the current loop gains K_p, K_i are properly chosen such that $V_p \in L_\infty$ and $\widetilde{\mathbf{i}} \in L_1$, then the following properties are satisfied: 1) the zero-state response yields

$$\bar{\epsilon}_Q \|\bar{\mathbf{e}}(t)\|_2 \le \alpha R_s(\kappa+1)\|\widetilde{\mathbf{i}}(t)\|_2$$

where $\bar{\mathbf{e}}(t) = [\,\tilde{x}(t) \quad \tilde{v}_m(t) \quad \widetilde{\lambda}^\top\,]^\top$ and $\bar{\epsilon}_Q = \min\{\alpha k_x, \alpha(D + k_v - \frac{\kappa c^2}{4R_s}), \frac{R_s}{L_s}(1 + L_m k_{\boldsymbol{\lambda}} - \frac{L_m^2}{4L_s\alpha})\}$; and 2) the asymptotic semi-current-fed LIM position control problem is solved, i.e., $\lim_{t\to\infty}\bar{\mathbf{e}}(t) = 0$.

V. Experimental Results

To further verify the validity of the proposed scheme, several experiments of speed and position control are described in this section. In our experiments, the developed controller is realized by a DSP-based control card (Simu-Drive system), which takes the TMS320F2812 DSP (fixed-point 32-bit) as the main control core. The DSP control card also provides multichannel of A/D and encoder interface circuits. Here, three-phase voltages and currents are sampled by the A/D converters and fed into the DSP-based controller. The speed and position are measured by a linear encoder with precision 20 μm for one pulse. In addition, the block-building MATLAB Simulink Toolbox and Real-Time Workshop are taken as an interface between software and hardware. When the build-up controller block is established, the Real-Time Workshop plays the role of a compiler to transform

TABLE I
SPECIFICATION AND PARAMETERS OF THE LINEAR INDUCTION MOTOR

INDUCTION MOTOR	
RATED SPECIFICATION	
POLE PAIR	2
POWER	1 HP
VOLTAGE	240 V
CURRENT	5 A
POLE PITCH	0.0465 m
SECONDARY LENGTH	0.82 m
PARAMETERS	
R_p	13.2 Ω
R_s	11.78 Ω
L_p	0.42 H
L_s	0.42 H
L_m	0.4 H
M	4.775 kg
D	53 kg/s

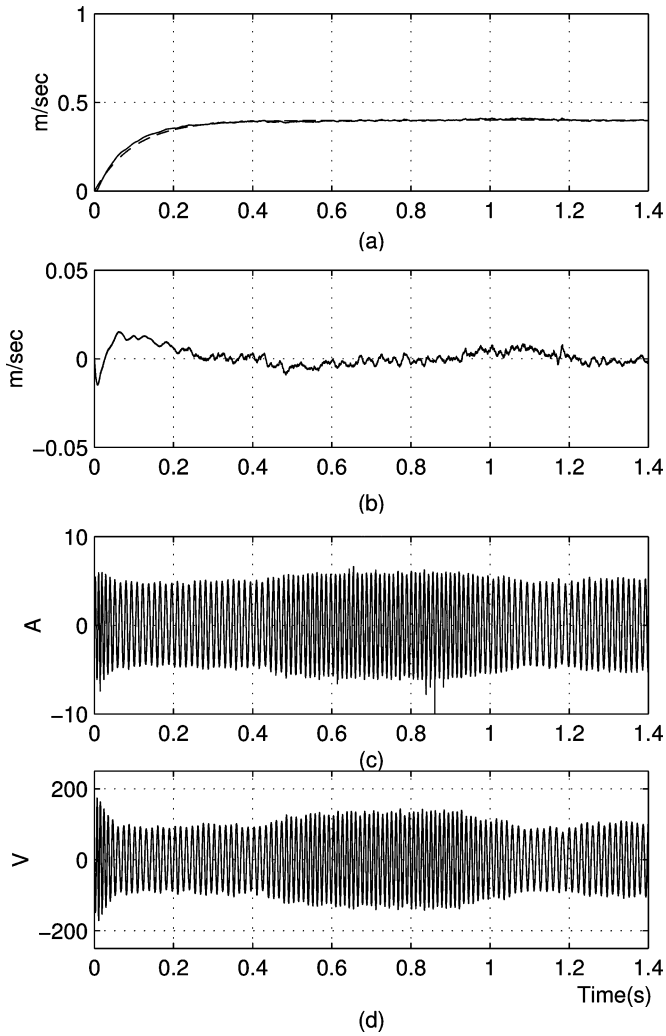

Fig. 3. Speed regulation with abrupt load variation. (a) Speed tracking response [reference (- - -), actual (—)]. (b) Speed tracking error. (c) Primary current of one phase. (d) Primary voltage of one phase.

the controller into a C code, which is download to the DSP-based control card. The specifications and parameters of the LIM are listed in Table I.

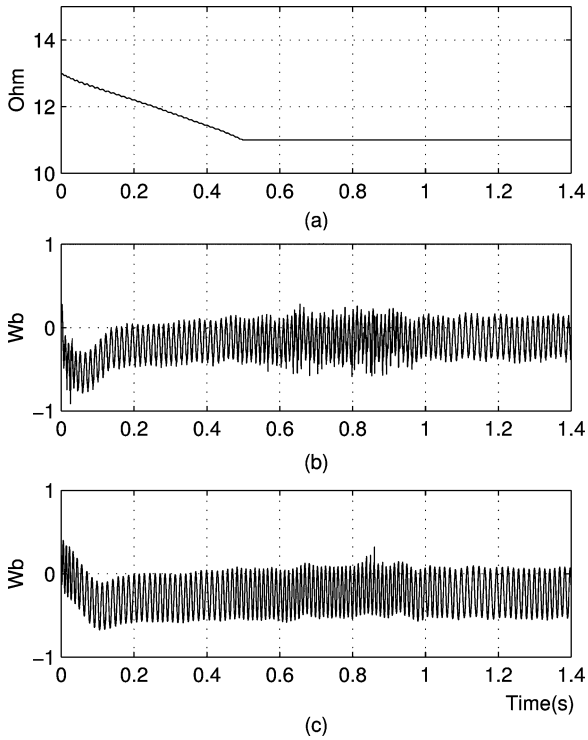

Fig. 4. Speed regulation with abrupt load variation. (a) Response of estimated secondary resistance. (b) and (c) Responses of estimated fluxes λ_{sa} and λ_{sb}.

A. Speed Control

The speed control parameters are chosen as follows: $K_p = 120, K_i = 30, \alpha = 0.045, k_v = 300.5, k_{\lambda} = 2.8$, and $c = 3.61$. Update gains are set to $\gamma_s = 0.1, \mathbf{\Gamma}_1 = \text{diag}\{10,\ 0.03,\ 0.001,\ 0.86,\ 0.03\}, \mathbf{\Gamma}_2 = \text{diag}\{0.1,\ 0.1\}, \mathbf{\Gamma}_3 = \text{diag}\{1.8,\ 1.8\}$. Based on this setting, the following speed control experiments are performed.

1) Experiment 1: Speed Regulation: Consider a speed regulation $v_d = 0.4$ m/s with an abrupt external force variation, where the external force 10 N is added at $t = 0.4$ s and removed at $t = 0.9$ s. The speed response resulting from the proposed controller (16) is shown in Fig. 3(a), while the speed tracking error is shown in Fig. 3(b). The primary current of u-phase, i_u and primary voltage of u-phase, V_u are shown in Fig. 3(c) and (d), respectively. Furthermore, the estimated secondary resistance and flux are illustrated in Fig. 4.

2) Experiment 2: Sinusoidal Speed Tracking: Consider the speed tracking command $v_d = 0.4 \sin 2\pi t$ m/s. The speed response resulting from the proposed controller (16) is shown in Fig. 5(a), while the speed tracking error is shown in Fig. 5(b). The primary current of u-phase, i_u and primary voltage of u-phase, V_u are shown in Fig. 5(c) and (d), respectively. All the estimated parameters and flux are bounded, but not shown here for space consideration.

3) Experiment 3: Triangular Speed Tracking: Consider a triangular speed command illustrated in Fig. 6(a). The speed response resulting from the proposed controller (16) is shown in Fig. 6(a), while the speed tracking error is shown in Fig. 6(b). The primary current of u-phase, i_u and primary voltage of u-phase, V_u are shown in Fig. 6(c) and (d), respectively.

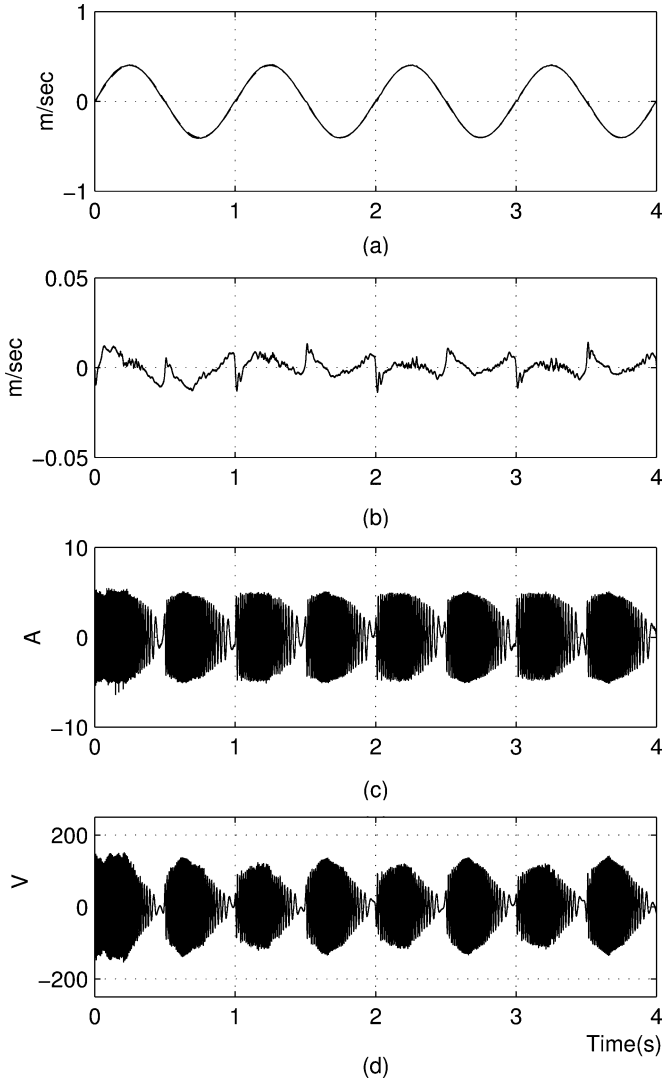

Fig. 5. Sinusoidal speed tracking. (a) Speed tracking response [reference (- - -), actual (—)]. (b) Speed tracking error. (c) Primary current of one phase. (d) Primary voltage of one phase.

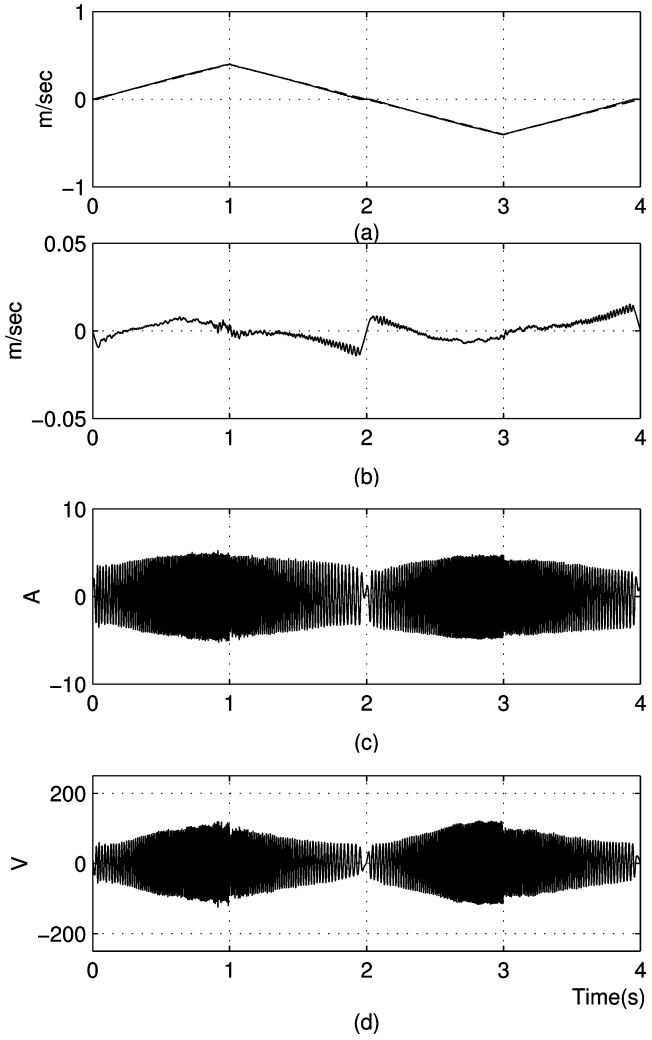

Fig. 6. Triangular speed tracking. (a) Speed tracking response [reference (- - -), actual(—)]. (b) Speed tracking error. (c) Primary current of one phase. (d) Primary voltage of one phase.

To emphasize that our approach is robust from a practical point of view, we also use a PI speed controller (a Simu-Drive system default PI) for the speed control objectives in Experiments 1 and 2. A comparison between the proposed controller and PI controller is shown in Fig. 7. In addition, to illustrate the effect of the end-effect compensation, we also apply the proposed controller with $\mathbf{\Gamma}_1 = \text{diag}\{10,\ 0,\ 0,\ 0.86,\ 0.03\}$ (which neglects the end-effect) for Experiment 3 and obtain the result shown in Fig. 8. Thus, a better performance is obtained by the proposed controller.

B. Position Control

The position control parameters are chosen as follows: $K_p = 120, K_i = 30, \alpha = 0.045, k_v = 300.5, k_{\lambda} = 2.8, k_x = 13$, and $c = 7.61$. Update gains are set to $\gamma_s = 0.1, \mathbf{\Gamma}_1 = \text{diag}\{10,\ 0.03,\ 0.001,\ 0.86,\ 0.03\}, \mathbf{\Gamma}_2 = \text{diag}\{0.1,\ 0.1\}$, and $\mathbf{\Gamma}_3 = \text{diag}\{1.8,\ 1.8\}$. Based on the controller setting, the following position control experiments are performed.

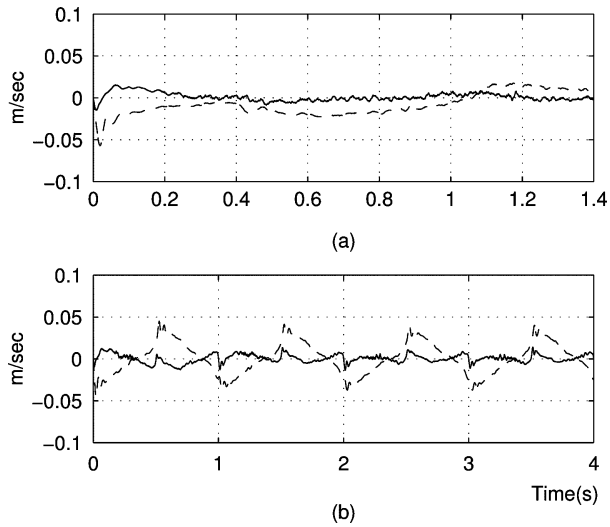

Fig. 7. Using PI (- - -) and proposed (—) speed controllers. (a) Error of speed regulation with abrupt load variation. (b) Error of sinusoidal speed tracking.

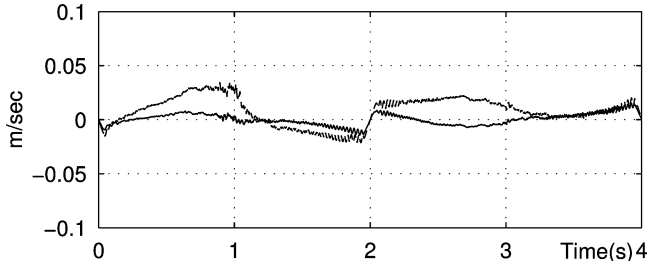

Fig. 8. Response of triangular speed tracking error under end-effect compensation (—) and without end-effect compensation (- - -).

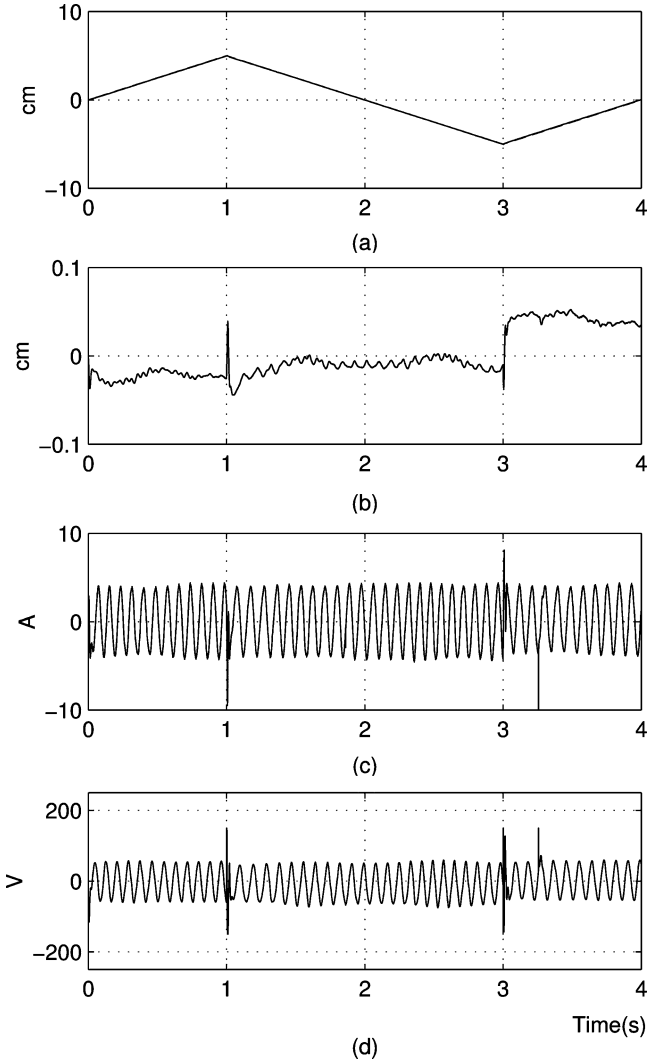

Fig. 9. Triangular position tracking. (a) Position tracking response [reference (- - -), actual(—)]. (b) Position tracking error. (c) Primary current of one phase. (d) Primary voltage of one phase.

1) Experiment 4: Triangular Position Tracking: Consider a triangular position command shown in Fig. 9(a). The proposed controller in Section IV yields the position tracking response shown in Fig. 9(a), while the position tracking error is shown in Fig. 9(b). The primary current of u-phase, i_u and primary voltage of u-phase, V_u are shown in Fig. 9(c) and (d), respectively.

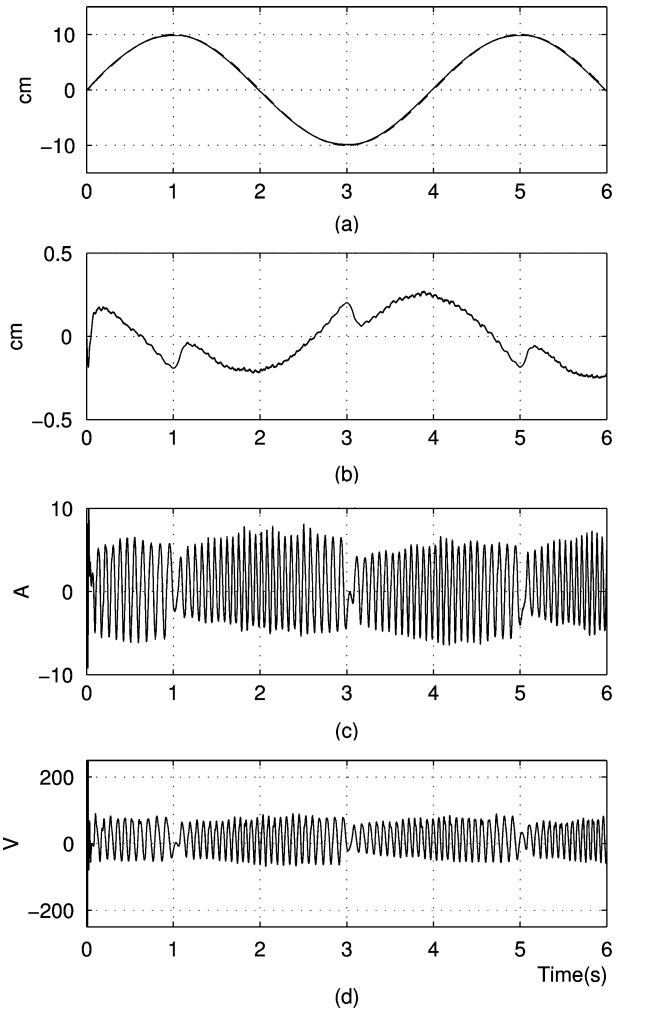

Fig. 10. Sinusoidal position tracking. (a) Position tracking response [reference (- - -), actual(—)]. (b) Position tracking error. (c) Primary current of one phase. (d) Primary voltage of one phase.

2) Experiment 5: Sinusoidal Position Tracking: Consider a position tracking command $x_d = 10 \sin \frac{\pi}{2} t$ cm. The position response is shown in Fig. 10(a), while the position tracking error is illustrated in Fig. 10(b). The primary current of u-phase, i_u and primary voltage of u-phase, V_u are shown in Fig. 10(c) and (d), respectively.

To illustrate the good performance of the proposed scheme, the Simu-Drive default PI controller is also applied to the triangular and sinusoidal position tracking. A comparison of the position tracking responses is shown in Fig. 11. It is apparent that both fast transient response and small steady-state error are obtained by the proposed controller.

Furthermore, to emphasize that our controller has great robustness, we purposely set the current loop gains as $K_p = 80$ and $K_i = 100$, which are far away from their own optimal values. Then, Experiments 4 and 5 are repeated. The experimental results compared with the original are illustrated in Fig. 12. The small difference on the responses indicates that the proposed scheme can tolerate the current-loop controllers which are not well tuned.

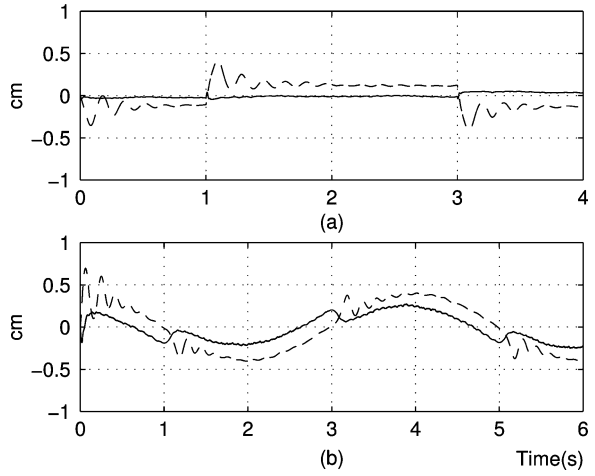

Fig. 11. Using PI (- - -) and proposed (—) position controllers. (a) Error of triangular position tracking. (b) Error of sinusoidal position tracking.

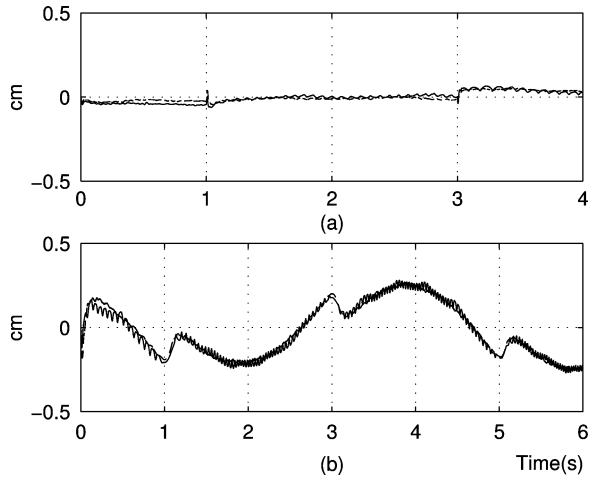

Fig. 12. Comparison of using optimal setting (- - -) and bad setting (—) loop gains. (a) Error of triangular position tracking. (b) Error of sinusoidal position tracking.

VI. Conclusion

Considering practical current-fed LIMs, we have successfully developed novel adaptive control schemes for speed and position tracking in this paper. Based on the problem formulation, the semi-current-fed LIM allows nonzero current error and hence, relaxes the ideal current loop assumption made in typical current-fed model. On the other hand, the benefit of a design using a reduced model is still preserved. Due to the high nonlinearity and nonzero current error, the VDV-based backstepping design has been introduced and provides asymptotic speed and position tracking without needing extra conditions. Furthermore, the effect from the current error to speed/position errors is attenuated to a prescribed level by appropriate control gains, i.e., L_2-gain control performance can be obtained even if the current loop control is not good enough. In addition, the flux tracking is achieved when the persistent excitation condition is satisfied. The experimental results have shown better tracking performances compared with the traditional control scheme.

Appendix I

In this appendix, we provide explicit derivation of equation (15):

$$\begin{aligned}\dot{\tilde{\lambda}} &= \dot{\widehat{\lambda}} - \dot{\lambda}_d \\ &= \dot{\eta} - \sigma\dot{\mathbf{i}} + \dot{\widehat{\mathbf{c}}}_0 - \dot{\lambda}_d \\ &= \dot{\lambda} + \dot{\widehat{\mathbf{c}}}_0 - \dot{\lambda}_d \\ &= \left(\frac{\pi}{\ell} n_p v_m \mathbf{J}_2 - \frac{R_s}{L_s}\mathbf{I}_2\right)\lambda + \frac{L_m R_s}{L_s}\mathbf{i} + \dot{\widehat{\mathbf{c}}}_0 - \dot{\lambda}_d\end{aligned}$$

Since $\lambda = \widehat{\lambda} + \widetilde{\mathbf{c}}_0$ and $\widehat{\lambda} = \tilde{\lambda} + \lambda_d$, it follows that

$$\begin{aligned}\dot{\tilde{\lambda}} &= \left(\frac{\pi}{\ell} n_p v_m \mathbf{J}_2 - \frac{R_s}{L_s}\mathbf{I}_2\right)\left(\tilde{\lambda} + \lambda_d\right) + \left(\frac{\pi}{\ell} n_p v_m \mathbf{J}_2 \right. \\ &\quad \left. - \frac{R_s}{L_s}\mathbf{I}_2\right)\widetilde{\mathbf{c}}_0 + \frac{L_m R_s}{L_s}\tilde{\mathbf{i}} + \frac{L_m R_s}{L_s}\mathbf{i}^* + \dot{\widehat{\mathbf{c}}}_0 - \dot{\lambda}_d \\ &= \left(\frac{\pi}{\ell} n_p v_m \mathbf{J}_2 - \frac{R_s}{L_s}\mathbf{I}_2 - \frac{R_s L_m k_\lambda}{L_s}\mathbf{I}_2\right)\tilde{\lambda} + \frac{\widetilde{R}_s L_m k_\lambda}{L_s}\tilde{\lambda} \\ &\quad + \frac{\widehat{R}_s L_m k_\lambda}{L_s}\tilde{\lambda} + \left(\frac{\pi}{\ell} n_p v_m \mathbf{J}_2 - \frac{\widehat{R}_s}{L_s}\mathbf{I}_2\right)\lambda_d - \frac{\widetilde{R}_s}{L_s}\lambda_d \\ &\quad + \frac{\pi}{\ell} n_p v_m \mathbf{J}_2 \widetilde{\mathbf{c}}_0 - \frac{R_s}{L_s}\mathbf{c}_0 + \frac{\widetilde{R}_s}{L_s}\widehat{\mathbf{c}}_0 + \frac{\widehat{R}_s}{L_s}\widehat{\mathbf{c}}_0 \\ &\quad + \frac{L_m R_s}{L_s}\tilde{\mathbf{i}} + \frac{L_m \widetilde{R}_s}{L_s}\mathbf{i}^* + \frac{L_m \widehat{R}_s}{L_s}\mathbf{i}^* + \dot{\widehat{\mathbf{c}}}_0 - \dot{\lambda}_d.\end{aligned}$$

Appendix II

Proof of Result for the Robust Speed Control

Consider the inequality (25) again and rewrite it as

$$\dot{V} \le -\varepsilon_e \|\mathbf{e}\|^2 + \varepsilon_i \|\tilde{\mathbf{i}}\| \|\mathbf{e}\|$$

where $\varepsilon_e = \min(\alpha(D + k_v), \frac{R_s}{L_s}(1 + L_m k_\lambda))$; and $\varepsilon_i = \sup_t \|[\alpha\kappa \mathbf{J}_2 \lambda_d \frac{L_m R_s}{L_s}\mathbf{I}_2]\| < \infty$ dependent on bounded parameters c, L_s, L_m, and R_s. If the current loop controller (5) performs well such that $\mathbf{V}_p \in L_\infty$ (i.e., $\tilde{\mathbf{i}} \in L_\infty$), then V is upper bounded due to $V > 0$ and $\dot{V} \le 0$ for $\|\mathbf{e}\| \ge \varepsilon_i \|\tilde{\mathbf{i}}\|/\varepsilon_e$. Hence the error signals $\tilde{v}_m$ and $\tilde{\lambda}$ are uniformly bounded. In other words, v_m, $\widehat{\lambda} \in L_\infty$ and all parametric errors $\widetilde{R}_s, \widetilde{\mathbf{c}}_0, \tilde{\vartheta}$ and $\tilde{\theta} \in L_\infty$. Due to $\lambda = \widehat{\lambda} + \widetilde{\mathbf{c}}_0$ and $\widehat{\lambda}, \widetilde{\mathbf{c}}_0 \in L_\infty$, the secondary flux λ is therefore uniformly bounded. The remaining thing is to investigate the boundedness of signals $\mathbf{i}^*$ and $\dot{\rho}(t)$. Let us rewrite the dynamics of the current (1) in the form

$$\sigma\dot{\mathbf{i}} + \left(\frac{L_s R_p}{L_m} + \frac{L_m R_s}{L_s}\right)\mathbf{i} = -\left(\frac{\pi}{\ell} n_p v_m \mathbf{J}_2 - \frac{R_s}{L_s}\mathbf{I}_2\right)\lambda + \frac{L_s}{L_m}\mathbf{V}_p$$

From the fact $v_m, \lambda, \mathbf{V}_p \in L_\infty$, the above equation is taken as a stable filter driven by a bounded input. This implies that the state $\mathbf{i}$ is uniformly bounded. Thus, the fact $\tilde{v}_m, \tilde{\lambda}, \mathbf{i} \in L_\infty$ ensures that $\mathbf{i}^*, \dot{\rho}(t)$, update laws $\widehat{R}_s, \widehat{\theta}, \widehat{\mathbf{c}}_0, \widehat{\vartheta}$, and auxiliary $\tau_\mathbf{a}$ are uniformly bounded. Finally, from the above analysis, we conclude that all signals on the right-hand sides of (18) and (19) are bounded in L_∞, which means $\mathbf{e}$ and $\dot{\mathbf{e}}$ are uniformly bounded. In addition,

since we only need selecting $\widehat{R}_s(0) > R_0$ for the update law (24), the boundedness is concluded in a global manner.

Furthermore considering (25) and facts

$$\alpha\kappa\tilde{v}_m\widetilde{\mathbf{i}}^\top\mathbf{J}_2\lambda_d \le \frac{\alpha\kappa c^2}{4R_s}\tilde{v}_m^2 + \alpha\kappa R_s\widetilde{\mathbf{i}}^\top\widetilde{\mathbf{i}}$$

$$\frac{L_m R_s}{L_s}\widetilde{\mathbf{i}}^\top\widetilde{\lambda} \le \frac{L_m^2 R_s}{4L_s^2\alpha}\widetilde{\lambda}^\top\widetilde{\lambda} + \alpha R_s\widetilde{\mathbf{i}}^\top\widetilde{\mathbf{i}},$$

we are able to rewrite $\dot{V}$ as

$$\begin{aligned}\dot{V} &\le -\alpha\left(D + k_v - \frac{\kappa c^2}{4R_s}\right)\tilde{v}_m^2 - \frac{R_s}{L_s}\left(1 + L_m k_\lambda\right. \\ &\quad \left. - \frac{L_m^2}{4L_s\alpha}\right)\widetilde{\lambda}^\top\widetilde{\lambda} + \alpha R_s(\kappa+1)\|\widetilde{\mathbf{i}}\|^2 \\ &= -\mathbf{e}^\top\mathbf{Q}\mathbf{e} + \alpha R_s(\kappa+1)\|\widetilde{\mathbf{i}}\|^2 \end{aligned} \tag{31}$$

where

$$\mathbf{Q} = \operatorname{diag}\left\{\alpha\left(D + k_v - \frac{\kappa c^2}{4R_s}\right), \frac{R_s}{L_s}\left(1 + L_m k_\lambda - \frac{L_m^2}{4L_s\alpha}\right)\mathbf{I}_2\right\}.$$

Note that $\mathbf{Q}$ is positive definite in accordance to properly chosen k_v, k_λ, and α from (26)–(28). Integrating on both sides of (31) leads to

$$\int_0^t \mathbf{e}^\top(\tau)\mathbf{Q}\mathbf{e}(\tau)d\tau \le V(0) + \alpha R_s(\kappa+1)\int_0^t \|\widetilde{\mathbf{i}}(\tau)\|^2 d\tau$$

and thus completes the proof.

REFERENCES

[1] I. Boldea and S. A. Nasar, *Linear Electric Actuators and Generators*. Cambridge, U.K.: Cambridge Univ. Press, 1997.

[2] I. Takahashi and Y. Ide, "Decoupling control of thrust and attractive force of a LIM using a space vector control inverter," *IEEE Trans. Ind. Appl*, vol. 29, no. 1, pp. 161–167, Jan./Feb. 1993.

[3] B. K. Bose, *Power Electronics and AC Drives*. Englewood Cliffs, NJ: Prentice Hall, 1986.

[4] S. A. Nasar and I. Boldea, *Linear Motion Electric Machines*. Hoboken, NJ: Wiley, 1976.

[5] V. H. Benitez, A. G. Loukianov, and E. N. Sanchez, "Neural identification and control of a linear induction motor using an $\alpha - \beta$ model," in *Proc. Amer. Control Conf.*, Denver, Colorado, Jun. 2003, pp. 4041–4046.

[6] C. I. Huang, K. O. Chen, H. T. Lee, and L. C. Fu, "Nonlinear adaptive backstepping motion control of linear induction motor," in *Proc. Amer. Control Conf.*, Anchorage, AK, May 2002, pp. 3099–3104.

[7] E. F. da Silva, C. C. dos Santos, and J. W. L. Nerys, "Field oriented control of linear induction motor taking into account end-effects," in *Proc. AMC'04*, Kawasaki, Japan, Mar., pp. 689–694.

[8] J. H. Sung and K. Nam, "A new approach to vector control for a linear induction motor considering end effects," *IEEE Ind. Appl. 34th IAS Annu. Meeting*, Phoenix, AZ, pp. 2284–2289, Oct. 1999.

[9] A. Gastli, "Improved field oriented control of an LIM having joints in its secondary conductors," *IEEE Trans. Energy Conver.*, vol. 17, no. 3, pp. 349–355, Sep. 2002.

[10] S. Vaez-Zadeh and M. R. Satvati, "Vector control of linear induction motors with end effect compensation," in *Proc. ICEMS*, Nanjing, China, Sep. 2005, pp. 635–638.

[11] N. Fujii and T. Harada, "Basic consideration of end effect compensator of linear induction motor for transit," *IEEE Ind. Appl. 35th IAS Annu. Meeting*, Rome, Italy, pp. 1–6, Oct. 2000.

[12] M. Salo and H. Tuusa, "A vector-controlled PWM current-source-inverter-fed induction motor drive with a new stator current control method," *IEEE Trans. Ind. Electron*, vol. 52, no. 2, pp. 523–531, Apr. 2005.

[13] C. C. de Wit and J. Ramirez, "Optimal torque control for current-fed induction motors," *IEEE Trans. Automat. Contr*, vol. 44, no. 5, pp. 1084–1089, May 1999.

[14] S. Peresada, A. Tilli, and A. Tonielli, "Theoretical and experimental comparison of indirect field-oriented controllers for induction motors," *IEEE Trans. Power Electron*, vol. 18, no. 1, pp. 151–163, Jan. 2003.

[15] W. J. Wang and J. Y. Chen, "Passivity-based sliding mode position control for induction motor drives," *IEEE Trans. Energy Convers.*, vol. 20, no. 2, pp. 316–321, Jun. 2005.

[16] L. Kumin, G. Stumberger, D. Dolinar, and K. Jezernik, "Modeling and control design of a linear induction motor," in *Proc. ISIE'99*, Bled, Slovenia, Jul., pp. 963–967.

[17] C. I. Huang and L. C. Fu, "Adaptive backstepping speed/position control with friction compensation for linear induction motor," in *Proc. IEEE Conf. Decision Control*, Las Vegas, NV, Dec.2002, pp. 474–479.

[18] K. Y. Lian, C. Y. Hung, C. S. Chiu, and P. Liu, "Induction motor control with friction compensation: An approach of virtual-desired-variable synthesis," *IEEE Trans. Power Electron*, vol. 20, no. 5, pp. 1066–1074, Sep. 2005.

[19] B. Karanayil, M. F. Rahman, and C. Grantham, "Stator and rotor resistance observers for induction motor drive using fuzzy logic and artificial neural networks," *IEEE Trans. Energy Convers*, vol. 20, no. 4, pp. 771–780, Dec. 2005.

[20] A. M. Lee, L. C. Fu, C. Y. Tsai, and Y. C. Lin, "Nonlinear adaptive speed and torque control of induction motors with unknown rotor resistance," *IEEE Trans. Ind. Electron*, vol. 48, no. 2, pp. 391–401, Apr. 2001.

[21] D. W. Novotny and T. A. Lipo, *Vector Control and Dynamics of AC Drives*. Oxford, U.K.: Clarendon, 1996.

[22] H. K. Khalil, *Nonlinear Systems*, 2nd ed. New York: Macmillan, 1996.

[23] M. Krstic, I. Kanellakopoulos, and P. Kokotovic, *Nonlinear and Adaptive Control Design*. New York: Wiley, 1995.

Kuang-Yow Lian (S'91–M'94) received the B.S. degree in engineering science from the National Cheng-Kung University, Tainan, Taiwan, R.O.C., in 1984 and the Ph.D. degree in electrical engineering from the National Taiwan University, Taipei, Taiwan, in 1993.

From 1986 to 1988, he served as an Assistant Researcher at Industrial Technology Research Institute (ITRI). From 1994–2007, he was an Associate Professor, Professor, and Chairman in the Department of Electrical Engineering, Chung-Yuan Christian University, Taiwan, R.O.C. He is also Chief Secretary General of the Chinese Automatic Control Society and Vice Chair of the IEEE Control System Society Taipei Chapter. His research interests include fuzzy control, nonlinear control systems, robotics, and control system applications.

Dr. Lian received the Outstanding Research Award from Chung-Yuan University, Chung-Li, Taiwan, in 2003.

Cheng-Yao Hung was born in Taipei, Taiwan, in 1978. He received the B.S. degree from the National Huwei Institute of Technology, Yunlin, Taiwan, R.O.C., in 2000, and the M.S. degree from Chung-Yuan Christian University, Chung-Li, Taiwan, in 2002, all in electrical engineering. He is currently working toward the Ph.D. degree in electrical engineering from Chung-Yuan Christian University, Chung-Li, Taiwan.

His current research interests include induction motor, linear induction motor, and nonlinear control theory.

Chian-Song Chiu (M'04) was born in Taiwan, R.O.C., in 1975. He received the B.S. degree in electrical engineering and the Ph.D. degree in electronic engineering from Chung-Yuan Christian University, Chung-Li, Taiwan, in 1997 and 2001, respectively.

Since 2003, he has been with the Department of Electronic Engineering, Chien-Kuo Technology University, Changhua, Taiwan, where he is currently an Associate Professor. He is the chapter coauthor of *Fuzzy Chaotic Synchronization and Communication—Signal Masking Encryption* (Soft Computing for Communication, New York: Springer-Verlag, 2004). His current research interests include fuzzy control, robotics, and nonlinear control.

Li-Chen Fu (S'85–M'88–SM'02–F'04) received the B.S. degree from the National Taiwan University, Taipei, Taiwan, R.O.C., in 1981, and the M.S. and Ph.D. degrees from the University of California, Berkeley, in 1985 and 1987, respectively.

Since 1987, he has been a member of the faculty, and is currently a Professor in both the Department of Electrical Engineering and the Department of Computer Science and Information Engineering, National Taiwan University, Taipei, Taiwan, where he currently serves as the Secretary General of the University. His research interests include robotics, FMS scheduling, shop floor control, home automation, visual detection and tracking, e-commerce, and control theory and applications. He has been the Editor of *Journal of Control and Systems Technology* and an Associate Editor of the prestigious control journal, *Automatica*. In 1999, he became the Editor-in-Chief of *Asian Journal of Control*.

Prof. Fu is a Senior Member of the IEEE Robotics and Automation and the IEEE Automatic Control Societies. He served as an AdCom Member of the IEEE Robotics and Automation Society during 2004–2005, the Program Chair of the IEEE International Conference on Robotics and Automation (ICRA) in 2003, and the Program Chair of the IEEE International Conference on Control Applications (CCA) in 2004.